

RESEARCH

Open Access



HnRNPM modulates alternative splicing in germ cells by recruiting PTBP1

Peng Lv^{1,2}, Wenchao Xu^{1,2}, Sheng Xin^{1,2}, Yuanxuan Deng^{1,2}, Bin Yang^{1,2}, Dengjianyi Xu^{1,2}, Jian Bai³, Deilin Ma⁴, Tao Wang^{1,2}, Jihong Liu^{1,2} and Xiaming Liu^{1,2*}

Abstract

Background Heterogeneous nuclear ribonucleoprotein M (HnRNPM) is a key splicing factor involved in various biological processes, including the epithelial–mesenchymal transition and cancer development. Alternative splicing is widely involved in the process of spermatogenesis. However, the function of hnRNPM as a splicing factor during spermatogenesis remains unknown.

Methods The expression of hnRNPM in germ cells at different stages was detected by polymerase chain reaction, western blotting, a single-cell database, and chromosome spreading assays. Conditional hnRNPM knockout mice were generated to observe the development of testes and germ cells in male mice. Histological staining, immunofluorescence staining and transmission electron microscopy were used to observe the abnormal development of sperm from conditional hnRNPM-deficient mice. Coimmunoprecipitation and mass spectrometry analyses revealed the proteins that interact with hnRNPM. RNA sequencing was performed to analyse the different alternative splicing events in the testes of control and hnRNPM-deficient mice.

Results In this study, we revealed that hnRNPM is highly expressed in spermatocytes and round spermatids, with the exception of XY bodies and metaphase. Therefore, we generated a germ cell-specific hnRNPM conditional knockout mouse model to investigate the role of hnRNPM in spermatogenesis. A lack of hnRNPM led to male infertility under natural conditions. Male hnRNPM-deficient mice presented lower numbers of sperm, lower motility, significantly more malformed sperm and even tailless sperm. Moreover, we found that hnRNPM interacted with PTBP1 to collectively regulate the process of spermatogenesis. In addition, we found that hnRNPM deficiency caused 1617 different alternative splicing events, and we detected abnormal exon skipping events in *Cep152*, *Cyld*, *Inpp4b* and *Cd59b*.

Conclusions Together, our results suggest that hnRNPM regulates the alternative splicing of mRNAs during spermatogenesis by recruiting PTBP1 and is required for male mouse fertility.

Keywords Male infertility, Spermatogenesis, HnRNPM, Alternative splicing

*Correspondence:

Xiaming Liu
xmliu77@hust.edu.cn

¹Department of Urology, Tongji Hospital, Tongji Medical College, Huazhong University of Science and Technology, Wuhan, Hubei, China
²Institute of Andrology, Tongji Hospital, Tongji Medical College, Huazhong University of Science and Technology, Wuhan, Hubei, China
³Reproductive Medicine Center, Tongji Hospital, Tongji Medical College, Huazhong University of Science and Technology, Wuhan, Hubei, China
⁴Department of Endocrinology, Tongji Hospital, Tongji Medical College, Huazhong University of Science and Technology, Wuhan, Hubei, China



© The Author(s) 2024. **Open Access** This article is licensed under a Creative Commons Attribution-NonCommercial-NoDerivatives 4.0 International License, which permits any non-commercial use, sharing, distribution and reproduction in any medium or format, as long as you give appropriate credit to the original author(s) and the source, provide a link to the Creative Commons licence, and indicate if you modified the licensed material. You do not have permission under this licence to share adapted material derived from this article or parts of it. The images or other third party material in this article are included in the article's Creative Commons licence, unless indicated otherwise in a credit line to the material. If material is not included in the article's Creative Commons licence and your intended use is not permitted by statutory regulation or exceeds the permitted use, you will need to obtain permission directly from the copyright holder. To view a copy of this licence, visit <http://creativecommons.org/licenses/by-nc-nd/4.0/>.

Background

Mammalian spermatogenesis is a complex and highly regulated process of germ cell proliferation and differentiation. This process can be broadly divided into the self-renewal of spermatogonia, meiosis of spermatocytes, morphological transition from round spermatids to elongated spermatids, and eventual maturation of spermatids [1]. Two extended periods of transcriptional inactivation have been discovered during the continuous process of gamete development. The first stage occurs in early meiosis, where spermatocytes undergo homologous recombination and crossing over. The second stage involves the transition from late elongating spermatids to mature spermatozoa and includes the halting of mRNA synthesis and the gradual cessation of translation [2–5]. In the phase of spermiogenesis, round spermatids undergo dramatic structural changes, including acrosome formation, nuclear chromatin condensation, flagellar aggregation, and the disposal of the remnant cytoplasm, which require the regulation of RNA binding proteins (RBPs) and alternative splicing (AS) to accommodate the complexity of the transcriptome. Owing to the transcriptional dynamics before chromatin condensation in spermiogenesis, alternative splicing, especially splicing variants, results in the production of large amounts of mRNA from a single gene and various protein isoforms that perform different functions [6, 7]. The regulatory function of alternative splicing plays crucial roles in the cellular response, cell differentiation and development [8]. Nuclear RBPs mainly process precursor mRNAs, including RNA modifications and alternative splicing. Moreover, cytoplasmic RBPs mainly regulate mRNA transport, controlling mRNA stability and interactions with the translational machinery [9]. Recently, more studies have indicated that RBPs participate in the precise posttranscriptional regulation of dynamic gene expression during spermatogenesis [10, 11].

The heterogeneous nuclear ribonucleoprotein (hnRNP) family, a large group of RNA binding proteins named A to U, consists of more than 20 hnRNP members [12]. Importantly, some hnRNPs are highly expressed in male mouse germ cells and have been identified as key regulators of male fertility [13]. A deficiency of hnRNPU in mouse Sertoli cells leads to male infertility, which is characterized by severely withered testes, a dramatic loss of Sertoli cells and germ cells, and the abnormal development and migration of spermatogonia during prepuberty. Moreover, the loss of hnRNPU in mouse germ cells in the embryonic stage causes abnormalities in the establishment of the spermatogonial stem cell pool and leads to aberrant alternative splicing [14, 15]. In addition, the loss of hnRNPK function in mouse germ cells causes atrophy of seminiferous tubules due to abnormal meiosis, which

manifests as arrest at the pachytene stage and the apoptosis of spermatocytes during spermatogenesis [16].

Researchers have described the complex effects of hnRNPM on the regulation of alternative splicing during the epithelial–mesenchymal transition [17]. Many studies have shown that altered expression of hnRNPM affects the growth and development of solid tumours, such as lung adenocarcinoma [18], Ewing sarcoma [19], hepatocellular carcinoma [20], gastric cancer [21] and breast cancer [22]. Moreover, sequencing results revealed that the binding function of hnRNPM differentially influences alternative splicing and the expression of transcripts in those tumours [18–20, 23]. However, the function of hnRNPM as a splicing regulator in spermatogenesis remains unknown.

In this study, we discovered that hnRNPM is highly expressed in spermatocytes and round spermatids, and that it mainly regulates the process of spermiogenesis. To investigate the critical role of hnRNPM in spermatogenesis, germ cell-specific hnRNPM conditional knockout mice were generated in the present study. In male mice, hnRNPM deficiency in the premeiotic stage significantly reduces fertility and increases the number of malformed spermatozoa. We further discovered that hnRNPM could recruit PTBP1 to regulate alternative splicing events. Interestingly, the RNA-seq analysis revealed that knocking out hnRNPM resulted in many aberrant alternative splicing events. This research highlights the crucial role of hnRNPM in normal spermiogenesis to maintain normal male fertility through the regulation of alternative splicing.

Methods

Animals

Floxed HnRNPM (Cyagen Biosciences, S-CKO-16606) and Stra8-EGFPcre (Cyagen Biosciences, C001283) mice on the C57BL/6J background were purchased from Cyagen Biosciences. Stra8-EGFPcre; hnRNPM^{flox/del} (SHCKO) mice were generated by mating Stra8-EGFPcre; hnRNPM^{flox/+} mice and hnRNPM^{flox/flox} mice. All the mice were bred at a constant room temperature (22–24 °C) with a humidity of 40–70% and a 12-hour light/dark cycle in a specific pathogen-free facility. We extracted genomic DNA from mouse toes to determine mice genotyping. The primer information is shown in Table 1.

Fecundity test

We assessed male fertility by mating 2-month-old Stra8-EGFPcre; hnRNPM^{flox/del} male mice with 2-month-old female wild-type C57BL/6J mice for six months. We recorded the number of offspring from each female mouse.

Table 1 Primer information in this study

Gene name	Sequence (5'-3')	Application
Gapdh	F: AGGTCGGTGTGAACGGATTTG R: GGGGTCGTGATGGCAACA	RT-PCR
Tubulin	F: TACACCAACCTTAACCGCCT R: GCTGCTCATGGTAGGCTTTC	RT-PCR
HnRNPM	F1: AAAGATGGGAAAAGTCGTGGAAT R1: GCATCGGTCTATCAAACAGCA F2: GAGCCATATTCCAACCCAACTAA R2: GCTCTCCTTGCAATGTTACC	RT-PCR
Cep152	F1: CCTTCCTGACTCCACCTCTG R1: CCCTCAGTGCCTCCAGTTTA	RT-PCR
Cyld	F1: CCCAGGTAGCAGGTTCCG R1: AGGAGCCACTAGTAAATCTGTCA	RT-PCR
Inpp4b	F1: ATCCTGAAAAGTGTCTGCCG R1: GTGGCTCGTTCCGAATCTTC	RT-PCR
Cd59b	F1: TGCCTGTTCCTTGGAT R1: TGCATGAAGAAACCGGTCTA	RT-PCR
HnRNPM	F: tagtccagtgtggtgaattcATGGCGGCAGGGGTCGAA R: atggtctttgtagtcctcgagAGCATTCTATCAATTCGAACATCA	Plasmid construction
Ptbp1	F: tagtccagtgtggtgaattcATGGACGGCATCGTCCCA R: tattagttttgttctcctcgagGATGGTGACTTGGAAAAGGAC	Plasmid construction
Stra8-EGFPcre	F1: GATGGATTCCGTCTCTGGTGAG R1: CCCATTTAATCTCCTCTTCTCCG F2: GTCAGAGAAGGTTGTATCGAACTGG	Genotyping
HnRNPM	F: TCACTGAACACCTGCCTTTTATT R: TCAAAGAGGGATAAGATGGCTCAG	Genotyping

Western blotting

Total protein was extracted with RIPA buffer (Beyotime Biotechnology, P0013J) containing a protease inhibitor cocktail (Servicebio, G2006). The lysates were clarified by centrifugation at $12,000 \times g$ at 4°C to obtain the supernatants. After proteins were denatured by heating in boiling water, the samples were separated via SDS-PAGE and electrotransferred to polyvinylidene fluoride membranes. The membranes were subsequently blocked with 5% non-fat milk for 1 h. The membranes were incubated with a primary antibody overnight at 4°C and then incubated with a secondary antibody for 1 h at room temperature. The signals were amplified with an ECL Enhanced Plus Kit (Abclonal, RM00021P) and photographed with chemiluminescence imaging analysis system (Bio-Rad, USA). The antibody information is shown in Table 2.

Polymerase chain reaction (PCR)

We isolated total RNA with VeZol Reagent (Vazyme, R411) and reverse transcribed it with a HiScript II Reverse Transcriptase Kit (Vazyme, R222). Quantitative real-time PCR (qRT-PCR) was performed with ChamQ Universal SYBR qPCR Master Mix (Vazyme, Q711) on Bio-Rad detection system called QuantStudio 6 Flex and software called QuantStudio™ Real-Time PCR v1.3.

Mouse Gapdh and Tubulin were used for internal normalization. The semiquantitative PCR products were analysed via agarose gel electrophoresis. The primer information is listed in Table 1.

Histological staining

Fresh testes and epididymides were immediately fixed with an improved Davidson's solution (mixture consisting of a 37% formaldehyde solution, glacial acetic acid and anhydrous ethanol) or 4% paraformaldehyde (Sigma, P6148) for 24 h. After dehydration and embedding in paraffin, $5 \mu\text{m}$ thick sections were obtained and placed on adhesive glass slides. Then, the sections were stained with haematoxylin (Servicebio, G1004) and eosin (HE) (Servicebio, G1001) or a periodic acid-Schiff (PAS) staining Kit (Beyotime Biotechnology, C0142S).

Immunofluorescence staining

The sections were heated in a microwave with a sodium citrate solution for antigen retrieval. The tissues were blocked with a 5% donkey serum solution for 1 h at room temperature. After washes with a phosphate buffer solution (PBS) (Servicebio, G0002), primary antibodies diluted in a 5% donkey serum solution were incubated with the samples overnight at 4°C . The sections were

Table 2 Information of reagents in immunofluorescence and Western blot

Antibody informations in this study			
Gene name	Company and Cat NO.	Application	concentration
HnRNPM	Abclonal (A20963)	WB	1:1000
		IF	1:100
		IP	10 µl/ml
Ddx4	Abcam (ab284611)	IF	1:200
PTBP1	Abclonal (A20963)	IF	1:200
		WB	1:1000
Sycp3	Santa cruz (sc-74569)	IF	1:200
Tubulin	Proteintech (66031-1-Ig)	WB	1:20000
HRP-conjugated Goat anti-Rabbit IgG	Abclonal (AS014)		1:500
HRP-conjugated Goat anti-Mouse IgG	Abclonal (AS003)		1:500
Coralite488-conjugated Goat Anti-Mouse IgG	Proteintech (SA00013-1)	IF	1:500
Coralite594-conjugated Goat Anti-Mouse IgG	Proteintech (SA00013-4)	IF	1:500
Flag tag	Proteintech (20543-1-AP)	IP	5 µl/ml
		WB	1:10000
Myc tag	Abmart (M20002)	IP	5 µl/ml
		WB	1:10000
Part of key reagents in immunofluorescence			
PNA	Maokangbio (MP6328)	IF	10 µg/ml
TUNEL kit	Elabscience (E-CK-A322)	IF	
DAPI	Beyotime (P0131)	IF	
TSA Fluorescence System Kit	RecordBio (RC0086-67R)	IF	

WB: Western blot; IF: Immunofluorescence; IP: Immunoprecipitation

subsequently washed with PBS and incubated with secondary antibodies for 1 h at room temperature. Finally, the sections were stained and mounted with Antifade Mounting Medium with DAPI (Beyotime Biotechnology, P0131). Images were acquired with a Lecia Application Suite X microsystem.

For TdT-mediated dUTP nick-end labelling, the deparaffinized sections are treated with proteinase K at 37 °C for half an hour. After three washes with PBS, we added TdT equilibration buffer and incubated the sections at 37 °C for half an hour. Then, we discarded the buffer, added the mixed labelling solution, and allowed it to react at 37 °C for 1 h. Finally, the sections were mounted with anti-fade mounting medium supplemented with DAPI.

For analyses of meiotic chromosome spread, fresh seminiferous tubules were incubated with hypotonic extraction buffer (30 mM Tris-HCl, 50 mM sucrose, 17 mM trisodium citrate dihydrate, 5 mM EDTA, 0.5 mM DTT, and 0.5 mM phenylmethylsulfonyl fluoride) for 30 min. We then separated single germ cells from seminiferous tubules and applied a thin layer on adhesive slides. After fixation with 1% paraformaldehyde containing 0.1% Triton-100, the samples were washed with Photo-Flo (Kodak, 1464510). The dried samples were blocked with 5% donkey serum solution and used for immunofluorescence staining.

For immunofluorescence staining of the sperm smear, we teared cauda epididymides and slightly blew on the mixture. We aspirated the solution and pushed it onto a

glass slide. Dried slides were fixed with a methanol solution and blocked with a 5% donkey serum solution for further immunofluorescence staining. All the staining reagents are shown in Table 2.

Epididymal sperm count, motility, and morphology

We dissected cauda epididymides from 3-month-old male mice that were quarantined for 3 days. Then, the cauda epididymides were gently torn, and we slightly shaken it in PBS to release the spermatozoa. The sperm solution and the counting plates were heated at 37 °C for 15 min before observation. The solution was diluted by a tenth and placed under a microscope for counting. We performed computer software-assisted measurements (BEION V4.90) to detect sperm motility and velocity. The slides of fresh sperm smears were prepared for morphological observation using a Diff-Quick Stain Kit with Fixative (Solarbio, G1540).

In vitro fertilization

Wild type female mice were injected with pregnant mare serum gonadotropin (Aibe Biotechnology, M2530) three days earlier and human chorionic gonadotropin (Aibe Biotechnology, M2520) two days earlier to induce superovulation. The cauda epididymides of male mice were acquired and incubated in human tubal fluid (Aibe Biotechnology, M1135) for 1 h. Then, the oocytes were collected and added to M2 medium (Aibe Biotechnology, M1250). Approximately 100 oocytes were added

to medium containing sperm and incubated for 6 h, after which all the oocytes were transferred into clean K+Simplex Optimized Medium (Aibei Biotechnology, M1435) for incubation at 37 °C for 18 h, after which two-cell embryos were counted as markers of normal insemination.

Transmission electron microscopy

Cauda epididymides were obtained from 3-month-old male mice and used to collect free sperm. The samples were fixed with a 2.5% glutaraldehyde solution (Solarbio, P1126) for 2 h at room temperature and then stored in a refrigerator at 4 °C. After fixation, the samples were washed with PBS three times and then postfixed with 1% OsO₄ (Ted Pella Inc, 18456) for 2 h. After dehydration, the samples were finally incubated with isoamyl acetate for 15 min. All the samples were dried in a dryer (Jinghong, DHG9140A) at 60 °C, attached to metallic grids and staining. The sperm structure was observed and imaged with a scanning electron microscope (Hitachi, HT7800).

Plasmid construction and cell transfection

We amplified the cDNA regions of hnRNPM and PTBP1 by PCR. We digested the vector plasmids (Miaoling Biology, P1003 and P0817) into fragments with the EcoRI and XhoI enzymes (Thermo Fisher Scientific, FD0274 and FD0694) for 10 min. We acquired the purified cDNAs of hnRNPM, PTBP1 and plasmid fragments using a V-ELUTE Gel Mini Purification Kit (Zoman, ZPV202-1). The hnRNPM cDNA was cloned and inserted into a pCMV vector containing the N-terminal Flag epitope tag, and the cDNA regions of Ptbp1 were cloned and inserted into a pCMV vector containing the N-terminal c-Myc epitope tag using the ClonExpress II One Step Cloning Kit (Vazyme, C112-01). The primers used are listed in Table 1. We subsequently transferred the cloning plasmids into DH5 α fast chemically competent cell (Yeasen, 11803ES80). The cloning plasmids were sequenced via Sanger sequencing (provided by Tsingke Biotech Co.) We amplified the bacterial solution containing the plasmid and acquired the plasmids via an Endo-free Plasmid Mini Kit II (OMEGA, D6950). HEK-293T cells were transfected with plasmids using Lipofectamine 3000 reagent (Thermo Fisher Scientific, L3000008) with DMEM medium containing 2% foetal bovine serum for 24 h, after which the medium was replaced with new DMEM supplemented with 5% foetal bovine serum for 36 h. The cells were collected for immunoprecipitation.

Immunoprecipitation

Mouse testes or cells were homogenized via iron bead (Servicebio, G0101-200G) disruption in cell lysis buffer. After being lysed on ice for 30 min, the lysates were

clarified by centrifugation at 12,000 \times g. Then, the supernatants were mixed with the relevant antibodies on a shaker overnight at 4 °C. Thereafter, we added magnetic Protein A/G beads to the mixtures for 2 h at room temperature. The beads were washed with Cell Lysis Buffer for Western and IP (Beyotime, P0013) and used for immunoprecipitation–mass spectrometry (IP-MS). The proteins were incubated with 5 mM dithiothreitol at 56 °C for 30 min, and then 11 mM iodoacetamide was added and incubated for 15 min at room temperature. Trypsin was added for the first digestion overnight at a 1:50 trypsin-to-protein mass ratio and then for the second digestion at a 1:100 ratio for 4 h. Finally, the peptides were desalted with a Strata X SPE column and analysed with a Bruker timsTOF Pro mass spectrometer. We analysed the interactions between of hnRNPM with other proteins via using UniProt [24] and STRING [25]. The antibodies used are listed in Table 2.

RNA-seq

As described above, total RNA was extracted from the testes of adult male mice. We tested the concentrations and quality of the samples with a NanoPhotometer spectrophotometer. A total of 2 μ g of RNA from each sample was used to establish cDNA libraries with the NEBNext® UltraTM RNA Library Prep Kit (Illumina, E3330). The quality of the libraries was subsequently detected using a Qubit 2.0 fluorometer and an Agilent 2100 bioanalyzer. The raw data were generated with the Illumina HiSeq 4000 platform. The reads were processed to remove adapters, N-containing reads and low-quality reads using Fastp (0.23.2). Clean data were paired with HISAT2 (v2.2.1). DESeq2 software (1.16.1) was used to perform the differential expression analysis between the two comparison combinations. The *P* values were adjusted using Benjamini and Hochberg's method. An adjusted *P* value < 0.05 and twofold changes were used as the thresholds. GO-GSEA and KEGG-GSEA of the differentially expressed genes were performed using clusterProfiler (v4.0) R software [26–28]. We used rMATS software to analyse the alternative splicing events between control and SHCKO testes, which included five main types of alternative splicing events: skipped exons (SEs), retained introns (RIs), mutually exclusive exons (MXEs), alternative 5' splice sites (A5SSs), and alternative 3' splice sites (A3SSs) [29]. A false discovery rate (FDR) < 0.05 and $|\Delta$ PSI| > 10% were categorized as differential alternative splicing events.

Statistical analysis

The data are presented as the means \pm standard deviations. GraphPad Prism 8.4 software and Excel software were used for the statistical analyses. A value of *p* < 0.05 was considered statistically significant for any differences.

p values are shown in the figures and figure legends: **p*<0.05, ***p*<0.01 and ****p*<0.001.

Results

hnRNPM is predominantly expressed in meiosis and round spermatids

To explore whether hnRNPM plays a key role in male reproduction, we first characterized the expression profile of hnRNPM in mice. The mRNA and protein levels of mouse hnRNPM were higher in mouse testes than in other organs (Fig. 1A and Supplementary Fig. S1A). Moreover, the hnRNPM mRNA and protein levels gradually began to increase at postnatal day 10 and reached the highest levels at postnatal day 28 (Fig. 1B and Supplementary Fig. S1B). To further explore its expression pattern during spermatogenesis, we used single-cell data from the Male Health Atlas database (<http://malehealthatlas.cn/>) to observe the mRNA expression of hnRNPM (Supplementary Fig. S1C) [30]. The results from the database revealed that the hnRNPM mRNA was expressed at low levels in spermatogonia and round spermatids, but was highly expressed in spermatocytes, and was almost completely absent in elongated spermatids. Next, we performed a chromosome spread assay to detect the subcellular location of hnRNPM in spermatocytes.

Consequently, the expression of hnRNPM was apparently lower in the leptotene stage, started to increase in the zygotene stage and was highly expressed from the pachytene stage to the diplotene stage, but was not detected in metaphase. However, we found that hnRNPM was absent in the region of the XY chromosome in the pachytene stage and diplotene stage (Fig. 1C). DDX4 is a putative marker for spermatogonia, spermatocytes and round spermatids in mouse testes. In addition, the immunofluorescence results revealed that hnRNPM was expressed in round spermatids, but its expression disappeared in elongated spermatids (Fig. 1D). These results suggest that hnRNPM plays a critical role in the process of male spermatogenesis.

hnRNPM is important for male fertility

To investigate the function of hnRNPM during spermatogenesis, we generated germ cell-specific knockout mice by deleting exons 3 to 5 of the hnRNPM gene with Stra8-EGFP-Cre (Fig. 2A). The genotype was identified via polymerase chain reaction and 2.5% agarose gel electrophoresis. The length of the gene containing the loxP site was 391 bp, and that of the wild-type gene was 323 bp (Fig. 2B). The length of the Stra8-EGFP-Cre gene was 443 bp, and that of the wild-type gene was

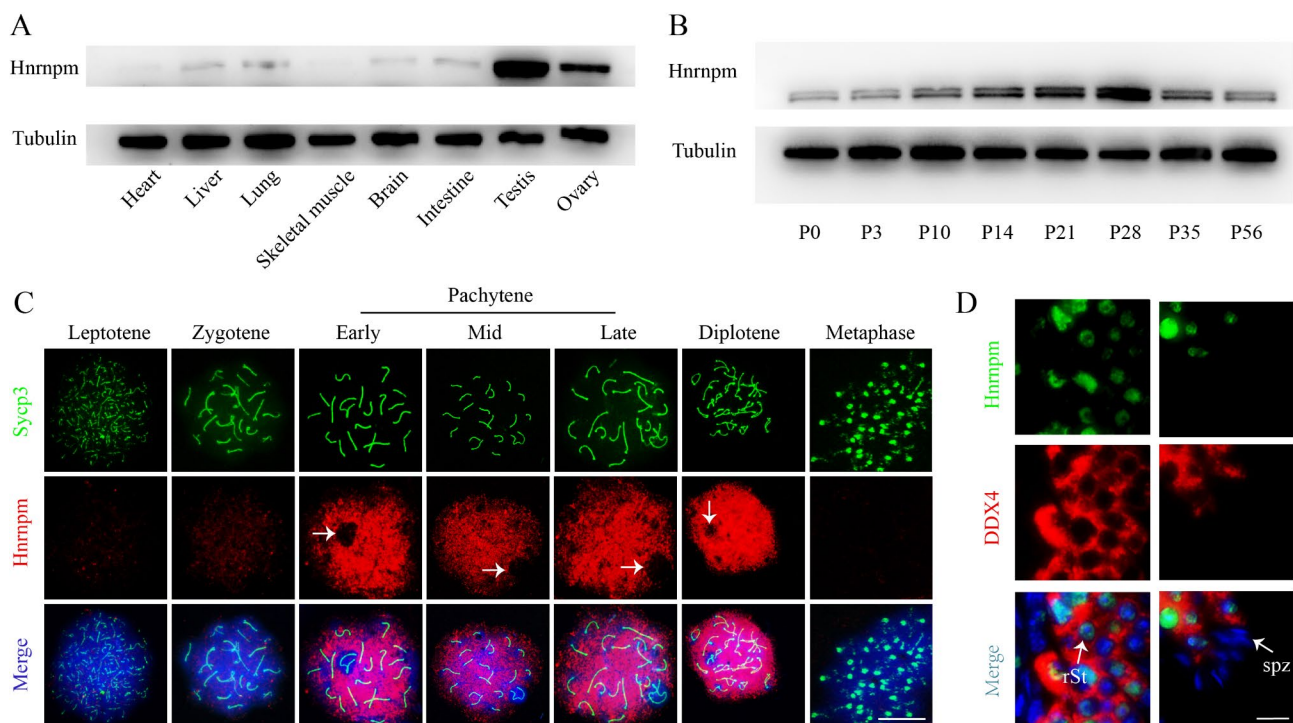


Fig. 1 hnRNPM shows a dynamic expression pattern in spermatogenesis. **A:** Expressions of hnRNPM protein in adult wildtype mouse multiple organs by Western blot. Tubulin was performed as control. Biologically independent mice ($n=3$) were tested in three separate experiments. **B:** Levels of hnRNPM protein in developing testes at postnatal day 0 (P0), P3, P10, P14, P21, P28, P35, and P56. Tubulin was performed as control. Biologically independent mice ($n=3$) were tested in three separate experiments. **C:** Double immunostaining with hnRNPM and Sycp3 on spermatocytes from wildtype adult mice were shown. The white arrows represent XY body. Scale bars = 5 μ m. **D:** Double immunostaining with hnRNPM and Ddx4 on tubules from WT adult mice were shown. Scale bars = 10 μ m

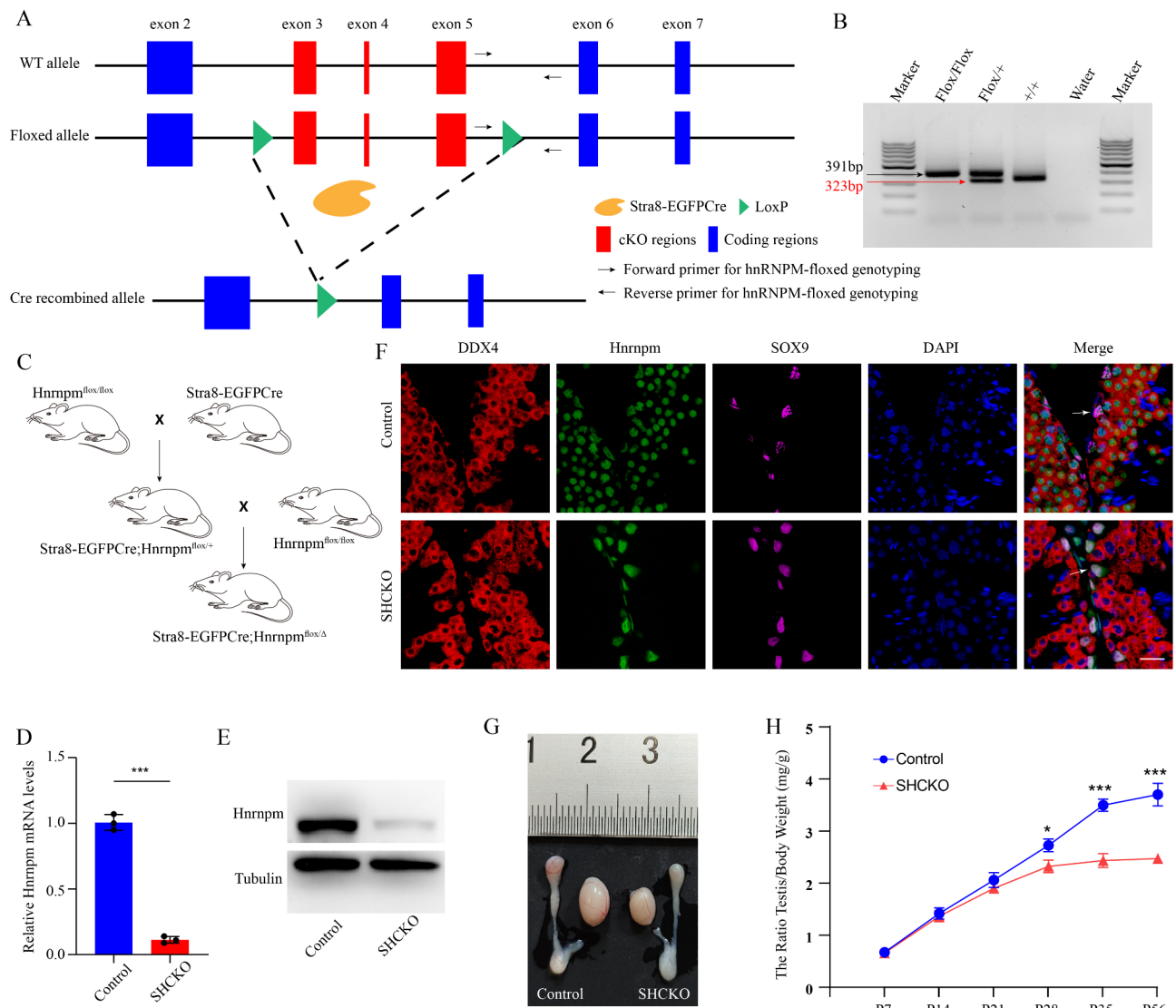


Fig. 2 hnRNPM ablation results in abnormal development of testes. **A:** Schematic diagram represents floxed hnRNPM allele to generate knockout allele by homologous recombination with cyclization recombination enzyme (Cre). We deleted exons 3 to exon 5 in germ cells. **B:** Genotyping images of tails from different mice, including flox/Del (or flox/flox), flox/+, and wild-type. **C:** Schematic diagram represents the generated procedure of hnRNPM knockout mouse with Stra8-EGFP-Cre. **D:** HnRNPM mRNA levels were analyzed by Real-time qPCR in control and hnRNPM knockout testes of postnatal day 21. Data were shown as mean \pm SD, $n=3$. T-test was performed. **E:** HnRNPM protein expressions were analyzed by western blot in control and hnRNPM knockout testes of postnatal day 21. Tubulin was performed as control. Biologically independent mice ($n=3$) were tested in three separate experiments. **F:** Immunofluorescence staining of hnRNPM, SOX9 and Ddx4 were performed in adult control and SHCKO mice. Scale bars = 20 μ m. **G:** Gross morphology of the testes and the epididymides from adult control and SHCKO mice. **H:** The development of testes in different postnatal controls and SHCKO mice were shown. Data were shown as mean \pm SD, $n=3$. T-test was performed

264 bp (Supplementary Fig. S1D). The process used to generate conditional knockout (cKO) mice is shown in Fig. 2C, and male Stra8-EGFP-Cre; HnRNPM^{+ /flox} mice were mated with female HnRNPM^{flox/flox} mice to obtain hnRNPM-deficient mice. The efficiency of hnRNPM deletion was detected using qRT-PCR and western blotting. The results revealed that hnRNPM expression was significantly lower in SHCKO mice compared with control mice at postnatal day 21 (Fig. 2D and E). Sox9 is a marker for Sertoli cells. Moreover, immunofluorescence

staining revealed that hnRNPM was undetectable in the nucleus of germ cells but was present in Sertoli cells in adult SHCKO mice compared with those in control mice (Fig. 2F). These results suggested that we succeeded in creating conditional germ cell-specific hnRNPM knockout mice.

After the SHCKO mice reached adulthood, we acquired testes from the control group and SHCKO group and found that the testes of the SHCKO group were apparently smaller than those of the control group

Table 3 Fertility test of male mice

	No. of males tested	No. of fertile males	Average pups per litters
Controls	5	5	8.067 ± 0.1756
SHCKO	5	0	0

(Fig. 2G). We subsequently analysed the ratio of testis weight to body weight in mice of different postnatal days. We observed a significant difference in the testis-to-body weight ratio on postnatal day 28. (Fig. 2H). Additionally, we found that the average pups of SHCKO male mice was 0 during the 6-month fecundity test, whereas it was 8.067 ± 0.1756 in the control animals (Table 3). These

results indicated that the loss of hnRNPM led to male sterility.

Deficiency of hnRNPM leads to abnormal spermatogenesis

Due to sharp sterility of SHCKO male mice, we performed HE staining and PAS staining to observe the seminiferous tubules and epididymis. Compared with those of the controls, the number of germ cells in the seminiferous tubules of the adult SHCKO male mice was significantly decreased at some specific stages and these cells were even absent in some of the tubules (Fig. 3A). In accordance with a series of developmental steps based on a fixed time schedule of spermatogenesis, we further discovered that adult SHCKO male mice underwent

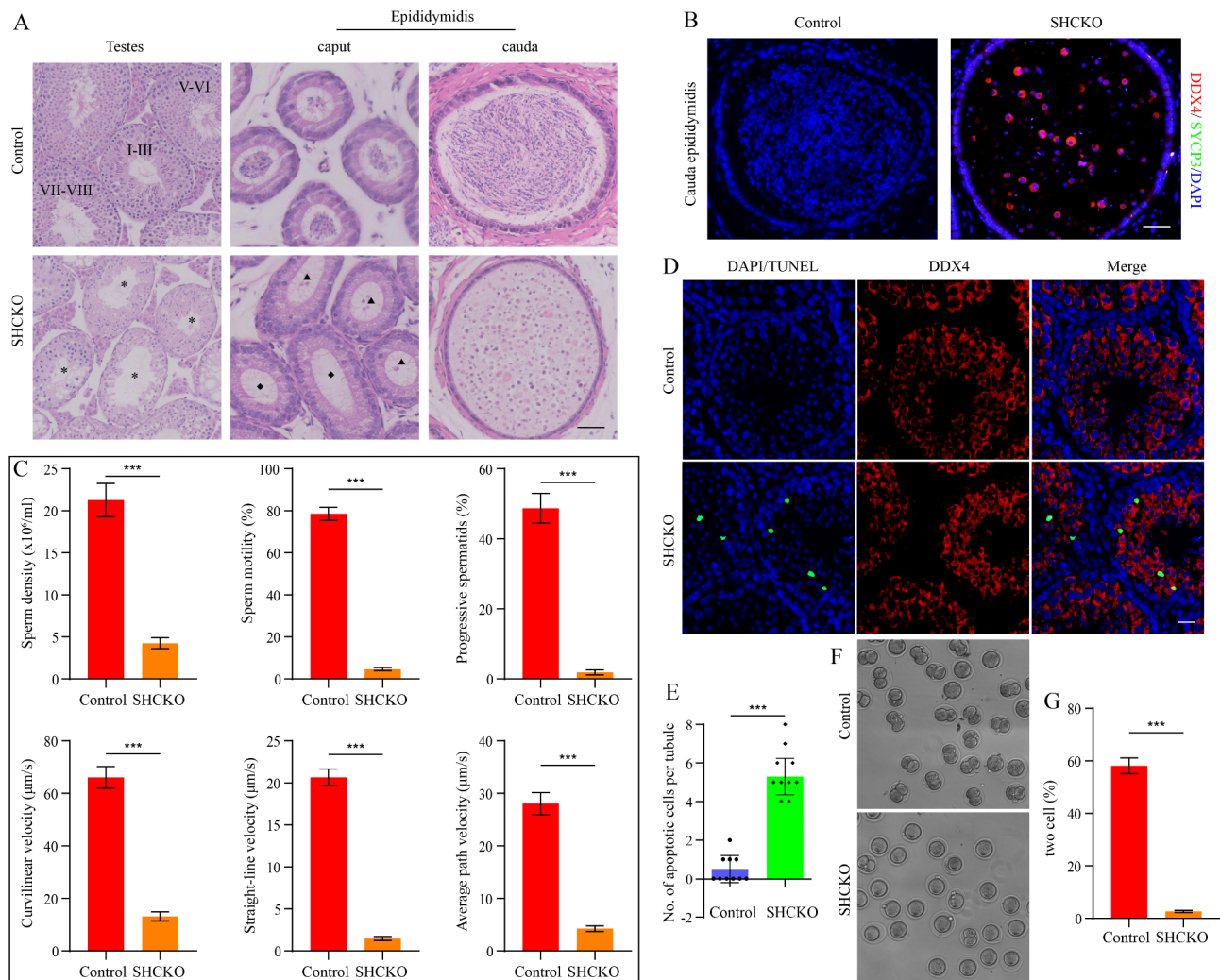


Fig. 3 hnRNPM is essential for male fertility. **A:** HE staining testes and epididymides from control and SHCKO mice at P56. Scale bars = 50 µm. **B:** Immunofluorescence staining of Sycp3 and Ddx4 were performed in control and SHCKO epididymides of adult mice. Scale bars = 50 µm. **C:** Sperm density, sperm motility, progressive spermatids, sperm curvilinear velocity, sperm straight line velocity, and sperm average path velocity of control and SHCKO mice. Data were shown as mean ± SD, n = 3. T-test was performed. **D:** TUNEL assay and DDX4 staining were performed to detect the apoptosis of testes from control and SHCKO mice. Scale bars = 20 µm. **E:** The numbers of apoptotic cells per tubules in control and SHCKO mice. **F:** In vitro fertilization was performed to examine the fertility of control and SHCKO mice. **G:** The two-cell embryo rate of control and SHCKO mice were shown. Data were shown as mean ± SD, n = 3. T-test was performed

complete procedure of spermatogenesis (Supplementary Fig. S2A). We found that germ cells were gradually lost at specific stages, such as the absence of round spermatids but the presence of spermatocytes and elongated spermatids, a lack of spermatocytes and round spermatids but the presence of elongated-like spermatids, or the loss of most germ cells with only a layer of cells observed (Supplementary Fig. S2B). Compared with those of the controls, we found many round cells in the epididymis of adult SHCKO male mice, and the number of sperm was strongly reduced (Fig. 3A). SYCP3 is a component of the synaptonemal complex and acts as a marker for meiosis I. Interestingly, IF staining showed DDX4-positive and SYCP3-negative cells in the cauda epididymis of adult SHCKO male mice, implying the presence of many round germ cells in the epididymis which shed from the seminiferous tubules before they matured (Fig. 3B). These results showed that the deletion of hnRNPM caused abnormal spermatogenesis.

The loss of hnRNPM in male germ cells leads to a severely decreased quantity and quality of sperm

Since SHCKO male mice do not have pups under natural conditions but do have elongated-like spermatids, we further performed sperm tests to identify the causes of infertility. First, we analysed the sperm density and motility via computer-assisted methods. Correspondingly, compared with those of control mice, the sperm density ($21.29 \pm 1.97 \times 10^6$ vs. $4.25 \pm 0.66 \times 10^6$), sperm motility ($78.61 \pm 3.13\%$ vs. $4.63 \pm 0.75\%$), progressive sperm rate ($48.74 \pm 4.23\%$ vs. $1.85 \pm 0.74\%$), sperm curvilinear velocity ($66.10 \pm 4.13 \mu\text{m/s}$ vs. $13.14 \pm 1.73 \mu\text{m/s}$), sperm straight line velocity ($20.67 \pm 0.99 \mu\text{m/s}$ vs. $1.48 \pm 0.23 \mu\text{m/s}$), and average sperm path velocity ($28.04 \pm 2.11 \mu\text{m/s}$ vs. $4.26 \pm 0.54 \mu\text{m/s}$) were all impaired in SHCKO mice. Compared with that in control mice, apoptotic germ cells were significantly increased in adult SHCKO male mice (Fig. 3D and E). These changes may contribute to the decreased numbers of germ cells. In addition, we performed IVF to detect the fertility of SHCKO male mice, and discovered that a very small number of spermatids from SHCKO male mice could fertilize eggs, and these eggs developed into two-cell embryos (Fig. 3F and G). We found that the proportion of two-cell embryos was $2.70 \pm 0.40\%$ in SHCKO male mice, whereas it was $58.18 \pm 3.00\%$ in the controls.

Sperm smear staining was performed using a Diff-Quik kit to observe the morphology of the sperm. We observed numerous sperm with abnormal morphologies of sperm in SHCKO male mice, mainly on abnormal head spermatids without tails or those with abnormal heads and thinner tails (Fig. 4A). PNA staining revealed many anomalous morphologies of the acrosome (Fig. 4B). In addition, transmission electron microscopy afforded

ultrastructural abnormalities in the sperm of SHCKO mice. Compared with those of the controls, we found that aberrant or irregular acrosomes were separated from the nucleus (Fig. 4C). Moreover, to determine whether the severely decreased motility and aberrant tails of spermatozoa was caused by a defective flagellar ultrastructure in SHCKO mice, we further applied transmission electron microscopy on the sperm flagellar ultrastructure. Transmission electron microscopy revealed that the diameter of the sperm in the SHCKO mice was smaller than that in the control mice (Fig. 4D). Moreover, an atypical “9+2” arrangement of axonemal microtubules and the outer dense fibres (ODFs) was observed in the midpiece and principal piece of the controls, but all of those arrangements were abnormal or absent in the sperm from the SHCKO mice. In the end piece, disordered peripheral microtubule doublets (MTDs) and disorganized central-pair microtubules (CPs) were apparent (Fig. 4D).

hnRNPM interacts with the splicing factor PTBP1

To illustrate how hnRNPM affects the development of germ cells, we performed immunoprecipitation mass spectrometry to identify candidate hnRNPM-interacting proteins in wild type mouse testes using an antibody of hnRNPM. Consequently, a total of 890 proteins were significantly different in the pulldown products, of which 255 proteins presented IP/IgG ratios greater than 2.5-fold (Fig. 5A). The Gene Ontology analysis revealed that 91 genes were enriched in the pathway of RNA splicing, 54 of which were involved in mRNA splicing based on UniProt annotations. In addition, the Kyoto Encyclopedia of Genes and Genomes enrichment analysis revealed that the top two pathways were the spliceosome and RNA degradation (Fig. 5B and C). Moreover, we found that 33 genes, including PTBP1, interacted with hnRNPM via the STRING database (Fig. 5D). We selected the splicing factor PTBP1 as a candidate protein that interacts with hnRNPM in the following ways: previous studies, IP/IgG ratios greater than twofold, GO and KEGG enrichment analyses and STRING analysis. PTBP1 has been shown to play a role as a key splicing factor in mouse spermatogenesis [31]. We further determined that PTBP1 interacted with hnRNPM in mouse testes at postnatal day 28 by performing coimmunoprecipitation assays (Fig. 5E). Moreover, the hnRNPM-Flag plasmid was cotransfected with the PTBP1-Myc plasmid in HEK-293T cells, and the interactions between hnRNPM and PTBP1 were confirmed by western blotting (Fig. 5F). Immunofluorescence staining revealed the colocalization of hnRNPM with PTBP1 in the germ cells, which supported the synergistic effect of hnRNPM with PTBP1 on the male reproductive system (Fig. 5G). These findings suggest that hnRNPM cooperates with the mRNA splicing factor

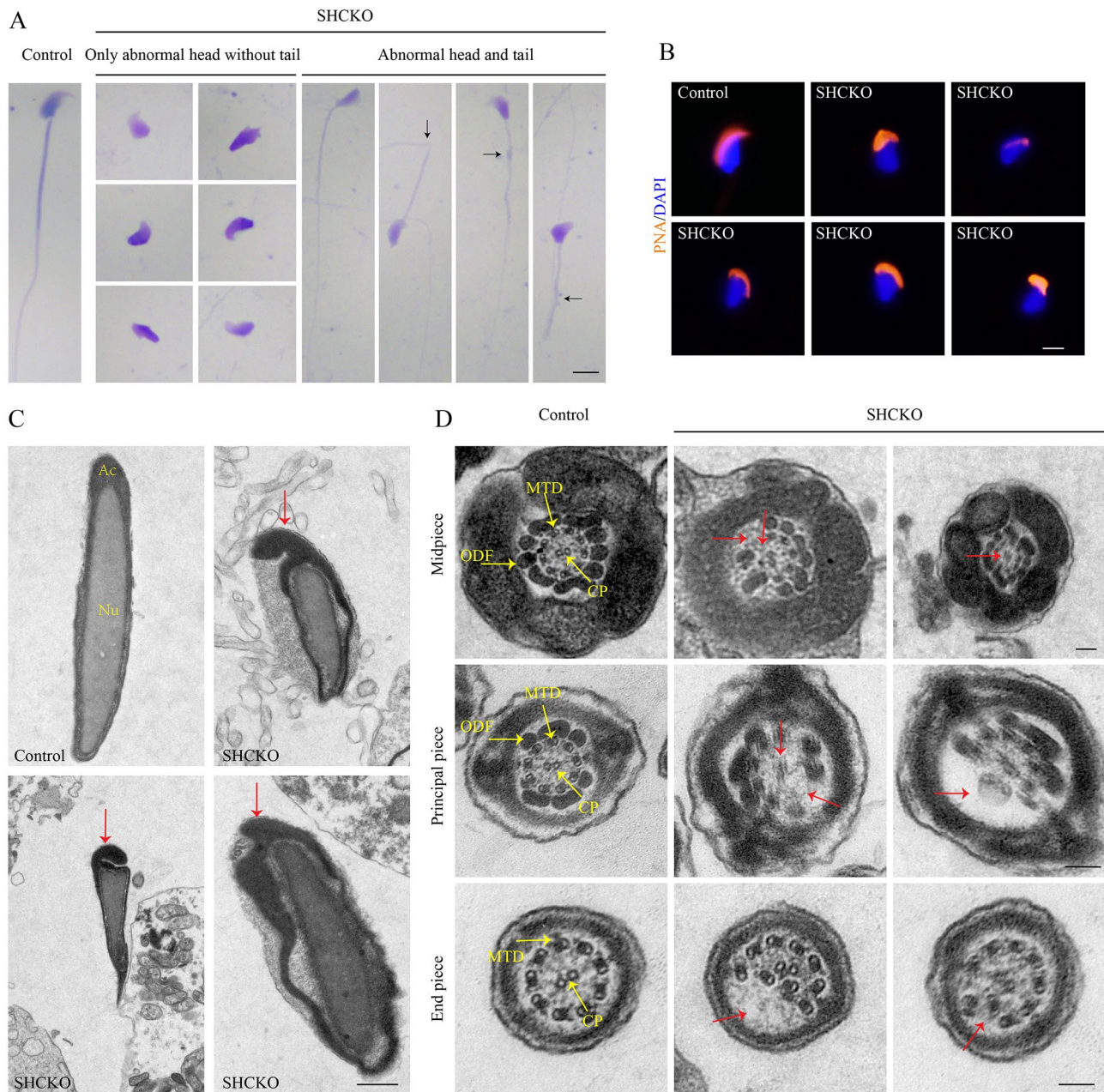


Fig. 4 loss of hnRNPM lead to abnormal morphology of sperm. **A:** The diff-quick stainings were performed in control and SHCKO mice. Scale bars = 20 μ m. **B:** Immunofluorescence staining of PNA were performed in adult control and SHCKO mice. Scale bars = 10 μ m. **C:** Transmission electron microscope of sperm heads from cauda epididymis of control and SHCKO mice. Ac: acrosome; Nu: nucleus. Red arrows represent abnormalities. Scale bar = 0.5 μ m. **D:** Transmission electron microscope of sperm flagella from cauda epididymis of control and SHCKO mice. ODF: outer dense fibers; MTD: peripheral microtubule doubles; CP: central-pair microtubules. Red arrows represent abnormalities. Scale bar = 100 nm

PTBP1 to affect the process of mRNA splicing during spermatogenesis.

The loss of hnRNPM results in aberrant alternative splicing in mouse testes

To better understand the molecular mechanism by which hnRNPM affects spermiogenesis, we performed RNA-seq on adult control and SHCKO mouse testes.

Compared with those in control mice, a total of 127 and 55 genes were identified as upregulated and downregulated, respectively, in SHCKO mice (Supplementary Fig. S3A). The GSEA-GO revealed that the differentially expressed genes were enriched mainly in axonemal dynein complex assembly, axoneme assembly and the sperm flagellum (Fig. 6A). Combined with previous studies showing that hnRNPM modulates alternative splicing

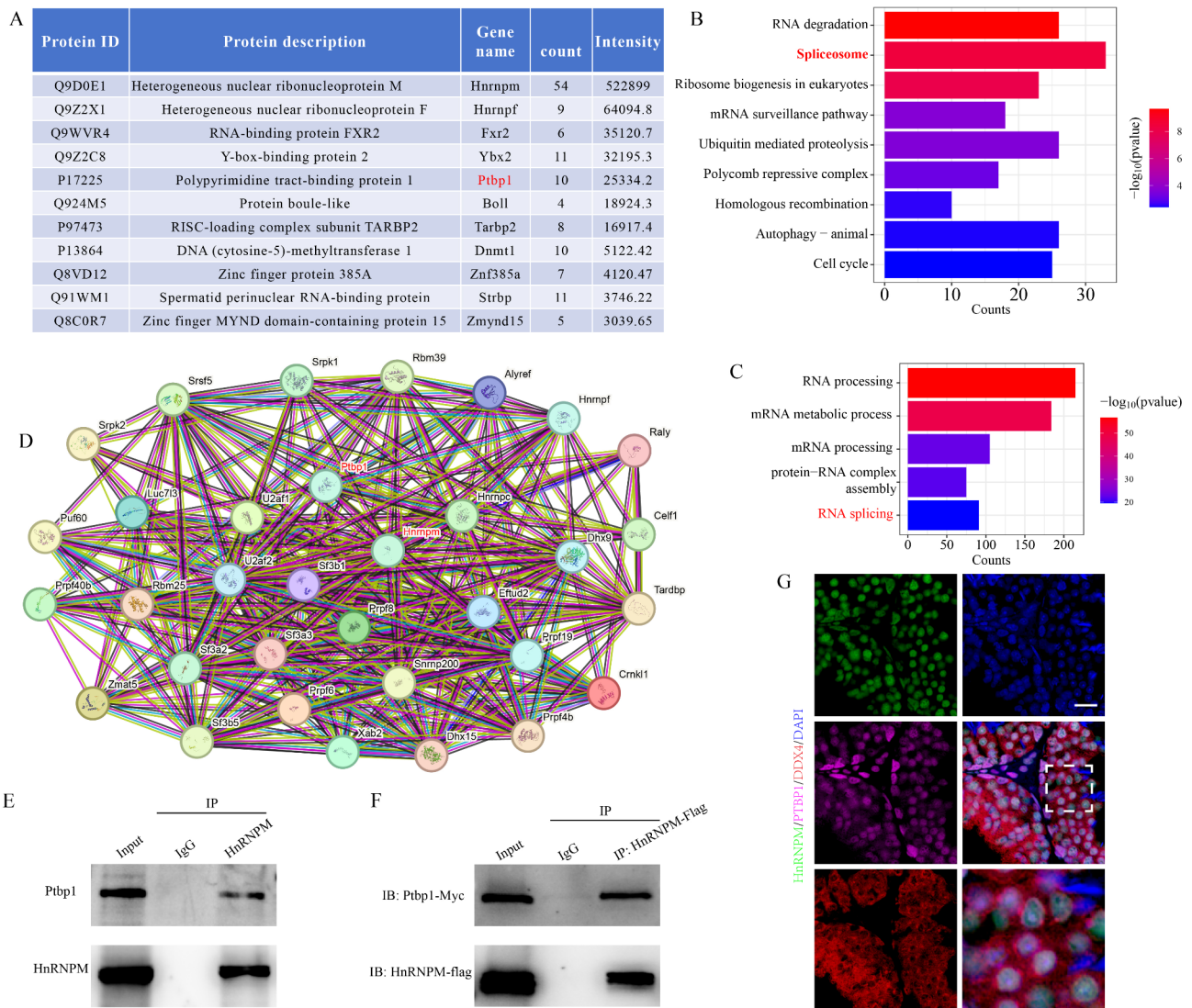


Fig. 5 hnRNPM interacts with splicing factor Ptbp1 in mouse testes. **A:** A table shows eleven proteins interact with hnRNPM, which are identified in adult wildtype mouse testes by IP-MS. **B:** KEGG enrichment analysis of hnRNPM-interacting proteins identified by IP-MS. **C:** GO enrichment analysis of hnRNPM-interacting proteins identified by IP-MS. **D:** The String analysis show the protein interaction networks among 33 candidate proteins associated with mRNA splicing (<http://cn.string-db.org>). **E:** Examination of interactions between hnRNPM and Ptbp1 in mouse testes by *in vivo* co-immunoprecipitation. IgG is used as control. **F:** Examination of interactions between hnRNPM and Ptbp1 by overexpression in 293T cells. IgG is used as control. **G:** Immunostaining with hnRNPM, DDX4 and PTBP1 in seminiferous tubules of wildtype adult mice. Scale bar = 20 nm

during the epithelial-mesenchymal transition and cancer metastasis, we performed an analysis of AS events in the RNA-seq data using rMATS software. Compared with those in control mice, the results identified a total of 1617 differential AS events in SHCKO mice, including alternative 5' splice site events, alternative 3' splice site events, mutually exclusive exon events, retained intron events, and skipped exon events (Fig. 6B). Subsequently, we performed a GO analysis of these different AS events. The results revealed that the enrichment of biological processes focused on mRNA processing, RNA splicing, and cilium organization (Supplementary Fig. S3B). The enrichment of molecular functions focused on tubulin

binding and microtubule binding (Supplementary Fig. S3C). The enrichment of cellular components focused on nucleus speck, which consists of large numbers of splicing factors, and microtubule (Supplementary Fig. S3D). We selected Cep152 and Cyld, which are related to axoneme formation and have been indicated to be indispensable for spermiogenesis [32, 33], to test the abnormal alternative splicing. Moreover, we selected Inpp4b and Cd59b which are involved in a decreased sperm count [34, 35]. Interestingly, the loss of hnRNPM in mouse testes caused increased exon inclusion of Cep152, increased exon inclusion of Cd59b, increased exon inclusion of Inpp4b, and increased exon skipping of Cyld (Fig. 6C and

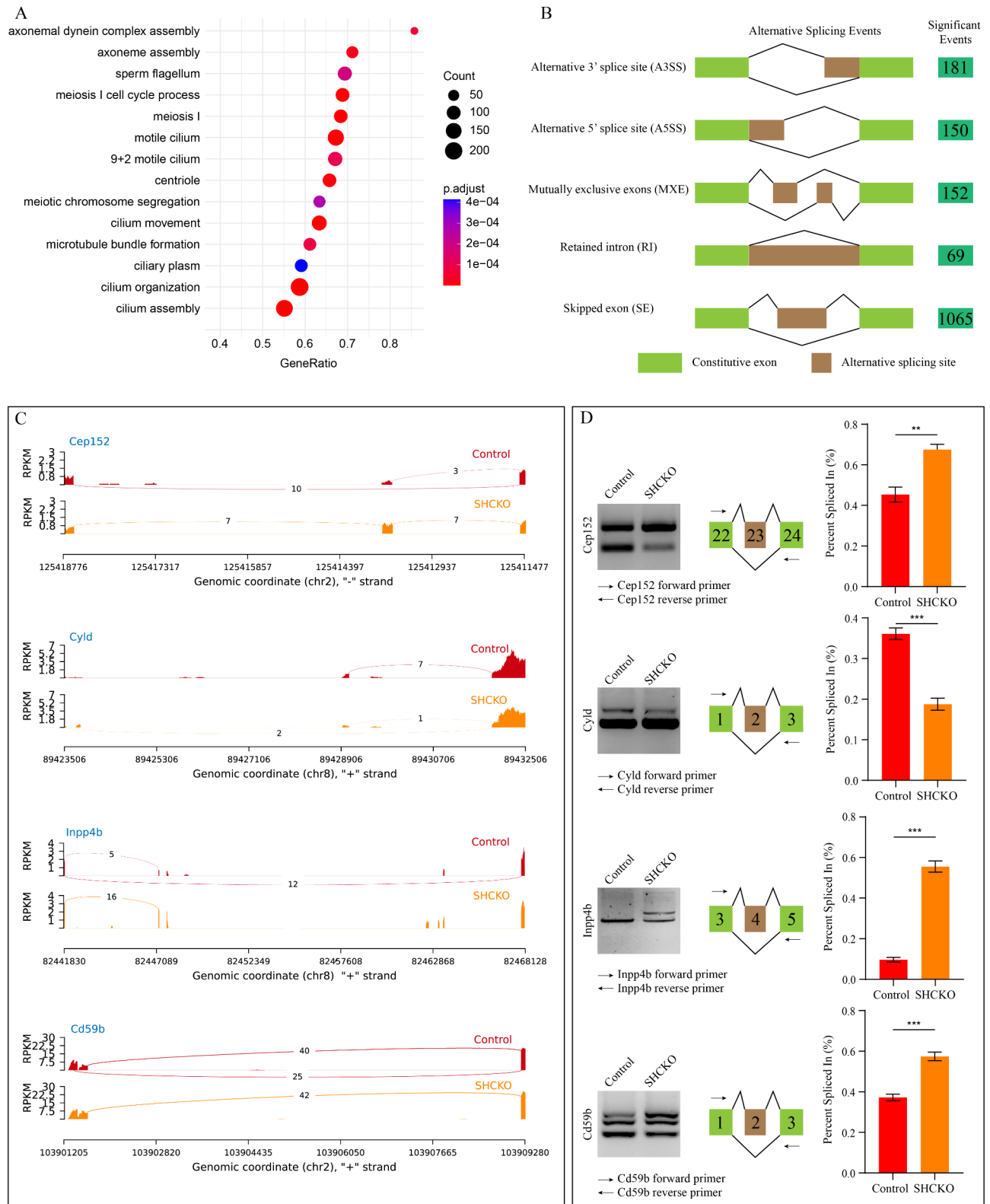


Fig. 6 Lack of hnRNPM cause aberrant alternative splicing in mouse testes. **A:** GESA-GO analysis of genes in control and SHCKO mice via RNA-seq. **B:** Number of alternative splicing events occurring in adult SHCKO mice. **C:** Sashimi plots of different alternative splicing events of selected genes (Cep152, Cyld, Inpp4b, and Cd59b) between control and SHCKO testes via RNA-seq. **D:** Examination of the selected candidate genes in control and SHCKO testes from 2-month-old mice. Data were shown as mean \pm SD, $n = 3$. T-test was performed

D). Taken together, these findings indicate that a lack of hnRNPM results in numerous aberrant alternative splicing events during spermatogenesis.

Discussion

Spermatogenesis is a highly coordinated process of germ cell differentiation that continuously generates normal mature sperm for male fertility. In this study, we first observed the essential role of hnRNPM in male fertility by generating germ cell-specific hnRNPM knockout mice. Overall, we revealed that the absence of hnRNPM induces multiple anomalies in sperm development, including the detachment of immature germ cells into the tubules, decreases in the sperm count and mobility, abnormalities in the formation of sperm acrosomes and defects in axonemes, which are consistent with the high expression time of hnRNPM. Hence, defining the specific function of hnRNPM during the process of spermatogenesis is difficult.

The hnRNPM-deficient male mice were mated with wild-type female mice but no pups were born under SPF conditions. Therefore, we originally thought that hnRNPM-deficient mice were infertile and completely unable to produce normal sperm. Moreover, we did not observe sperm with a normal morphology in the epididymal sections or sperm smears, further validating our idea. On the other hand, the presence of DDX4-positive and SCP3-negative round germ cells in the epididymis of hnRNPM knockout mice suggested impaired cell adhesion and junctions, which promoted the sloughing of immature germ cells to tubules and reduced the number of germ cells. Combining these results, we hypothesized that the decreases in both the number and quality of sperm in male hnRNPM-deficient mice ultimately led to sterility. However, we found that sperm from hnRNPM knockout mice successfully fertilized very few eggs from female wild-type mice through in vitro fertilization, suggesting that a very small amount of normal sperm were generated in hnRNPM-deficient male mice. According to clinical experience, some patients diagnosed with oligoasthenoteratozoospermia are unable to produce offspring during the natural mating process but need to rely on microdissection testicular sperm extraction techniques to obtain a very small amount of normal sperm to fertilize normal eggs, which may be similar to our results [36]. Due to a severe deficiency of normal sperm, we failed to observe normal spermatozoa in experiments assessing sperm morphology. More detailed observations of hnRNPM-deficient mice using electron microscopy revealed abnormalities in the formation of sperm acrosomes and axonemes, which suggested that the main cause of infertility is the large number of abnormal spermatozoa. Defects in the “9+2” arrangement of axonal microtubules and malformed acrosomes lead to a

loss of sperm motility and ability to penetrate the zona pellucida.

Through immunoprecipitation and immunofluorescence staining, we found that hnRNPM interacts with PTBP1 and colocalizes within the germ cell nucleus, which suggests that alternative splicing exerts great influence on the process of spermatogenesis. Similarly, germ cells showed increased apoptosis and the sperm count was significantly decreased in *Ptbp1*-deficient mice, as observed in hnRNPM-deficient mice [37]. Our results revealed that the ablation of hnRNPM resulted in a total of 1617 differential AS events in adult mouse testes, many of which regulated the formation of spermatids. However, the loss of PTBP1 results in delayed proliferation of spermatogonia followed by a gradual decrease in the sperm count, which differs from our results. Following the loss of PTBP1, the alternative splicing of 85 genes was altered, but none of the genes were differentially expressed in *Ptbp1*-knockout germline stem cells. We observed that many layers of germ cells were absent, leaving only one layer of cells within some seminiferous tubules from hnRNPM-deficient mice. This phenomenon may be related to the proliferation of spermatogonia, which is regulated by both hnRNPM and PTBP1, but research evidence is lacking. Whether PTBP1 and hnRNPM share a common regulatory mechanism remains unclear, although they are derived from the same protein superfamily. Future studies are necessary to determine the role of hnRNPM in spermatogonia.

Germ cells undergo substantial changes during spermiogenesis to form elongated spermatids [38]. The neck and long tail are essential for the motility of sperm. A head–tail coupling device is present in the region of the neck, which consists of a centrosome-based structure composed of two centrioles [39]. Moreover, a *Drosophila melanogaster* orthologue of Cep152 is required for axoneme formation in the sperm flagellum [33]. In the present study, we detected a significant increase in the level of exon 23 inclusion of Cep152 in hnRNPM-deficient germ cells, which contributed to abnormal axoneme formation. Differences in spermatogenesis exist between *Drosophila melanogaster* and mice, but our results indirectly provide more evidence for the function of Cep152 in mice. Future research on the role of alternative splicing variants of key genes during spermatogenesis will continue to be refined in mouse genetic models.

Conclusions

In summary, our explorations identify hnRNPM as a critical regulator of male fertility. Our study substantiated that hnRNPM is an important splicing factor associated with sperm formation in mice. Conditional knockout of the hnRNPM gene in male germ cells causes decreased sperm counts and motility, malformed acrosomes, a

chaotic arrangement of axonemes, and even tailless sperm. HnRNPM regulates the splicing events of precursor mRNAs associated with flagellar formation by interacting with PTBP1. The elucidated molecular mechanism underlying the role of hnRNPM in male spermiogenesis provides insights into the function of alternative splicing in male fertility. Further genetic testing of hnRNPM in infertile men may give more information to investigate the causes of male infertility, which could provide an avenue for therapeutic strategies for male infertility in humans.

Abbreviations

A3SS	Alternative 3' splice site
A5SS	Alternative 5' splice site
AS	Alternative splicing
CPs	Central-pair microtubules
hnRNP	Heterogeneous nuclear ribonucleoprotein
MTDs	Microtubule doublets
MXE	Mutually exclusive exons
ODFs	Outer dense fibers
PBS	Phosphate buffer solution
RBPs	RNA binding proteins
RI	Retained intron
SE	Skipped exon

Supplementary Information

The online version contains supplementary material available at <https://doi.org/10.1186/s12958-024-01340-5>.

Supplementary Material 1

Acknowledgements

The authors would like to thank all researchers who afforded previous studies, the Public Research Platform of Tongji Hospital, and all our friends.

Author contributions

Conceptualization: experimental design and funding, WT, LJH and LXM; manuscript drafting and editing, LP and LXM; experiments execution, LP; data collection, curation and analyses, LP, XWC, XS, DYX, YB and XDJY; validation, supervision and coordination, BJ, MDL and LXM.

Funding

This work was supported by the National Natural Science Foundation of China (82072838).

Data availability

All data supporting the findings of this study are included within the article and supplementary files. The requests of datasets or other data can be available from the corresponding authors, even provide it to the public websites.

Declarations

Ethics approval and consent to participate

All animal experiments have approved by the Institutional Animal Care and Use Committee of Tongji hospital, Tongji Medical College, Huazhong University of Science and Technology (IACUC Issue NO.: TJH-202212007).

Consent for publication

Not applicable.

Competing interests

The authors declare no competing interests.

Received: 10 September 2024 / Accepted: 21 December 2024

Published online: 08 January 2025

References

1. Neto FT, Bach PV, Najari BB, Li PS, Goldstein M. Spermatogenesis in humans and its affecting factors. *Semin Cell Dev Biol.* 2016;59:10–26.
2. Sassone-Corsi P. Unique chromatin remodeling and transcriptional regulation in spermatogenesis. *Science.* 2002;296:2176–8.
3. Idler RK, Yan W. Control of messenger RNA fate by RNA-binding proteins: an emphasis on mammalian spermatogenesis. *J Androl.* 2012;33:309–37.
4. Kleene KC. Connecting cis-elements and trans-factors with mechanisms of developmental regulation of mRNA translation in meiotic and haploid mammalian spermatogenic cells. *Reproduction.* 2013;146:R1–19.
5. Ernst C, Eling N, Martinez-Jimenez CP, Marioni JC, Odom DT. Staged developmental mapping and X chromosome transcriptional dynamics during mouse spermatogenesis. *Nat Commun.* 2019;10:1251.
6. Elliott DJ, Grellscheid SN. Alternative RNA splicing regulation in the testis. *Reproduction.* 2006;132:811–9.
7. Song H, Wang L, Chen D, Li F. The function of pre-mRNA alternative splicing in mammal spermatogenesis. *Int J Biol Sci.* 2020;16:38–48.
8. Marasco LE, Kornblihtt AR. The physiology of alternative splicing. *Nat Rev Mol Cell Biol.* 2023;24:242–54.
9. Corley M, Burns MC, Yeo GW. How RNA-binding proteins interact with RNA: molecules and mechanisms. *Mol Cell.* 2020;78:9–29.
10. Nguyen-Chi M, Morello D. RNA-binding proteins, RNA granules, and gametes: is unity strength? *Reproduction.* 2011;142:803–17.
11. Morgan M, Kumar L, Li Y, Baptissart M. Post-transcriptional regulation in spermatogenesis: all RNA pathways lead to healthy sperm. *Cell Mol Life Sci.* 2021;78:8049–71.
12. Geuens T, Bouhy D, Timmerman V. The hnRNP family: insights into their role in health and disease. *Hum Genet.* 2016;135:851–67.
13. Wang XL, Li JM, Yuan SQ. Characterization of the protein expression and localization of hnRNP family members during murine spermatogenesis. *Asian J Androl.* 2023;25:314–21.
14. Wen Y, Zhou S, Gui Y, Li Z, Yin L, Xu W, Feng S, Ma X, Gan S, Xiong M, et al. hnRNPU is required for spermatogonial stem cell pool establishment in mice. *Cell Rep.* 2024;43:114113.
15. Wen Y, Ma X, Wang X, Wang F, Dong J, Wu Y, Lv C, Liu K, Zhang Y, Zhang Z, Yuan S. hnRNPU in sertoli cells cooperates with WT1 and is essential for testicular development by modulating transcriptional factors Sox8/9. *Theranostics.* 2021;11:10030–46.
16. Xu H, Guo J, Wu W, Han Q, Huang Y, Wang Y, Li C, Cheng X, Zhang P, Xu Y. Deletion of Hnrnpk gene causes infertility in male mice by disrupting spermatogenesis. *Cells.* 2022;11.
17. Harvey SE, Xu Y, Lin X, Gao XD, Qiu Y, Ahn J, Xiao X, Cheng C. Coregulation of alternative splicing by hnRNPM and ESRP1 during EMT. *RNA.* 2018;24:1326–38.
18. Lee YF, Phua CZJ, Yuan J, Zhang B, Lee MY, Kannan S, Chiu YHJ, Koh CWQ, Yap CK, Lim EKH, et al. PARP4 interacts with hnRNPM to regulate splicing during lung cancer progression. *Genome Med.* 2024;16:91.
19. Passacantilli I, Frisone P, De Paola E, Fidaleo M, Paronetto MP. hnRNPM guides an alternative splicing program in response to inhibition of the PI3K/AKT/mTOR pathway in Ewing sarcoma cells. *Nucleic Acids Res.* 2017;45:12270–84.
20. Zhu GQ, Wang Y, Wang B, Liu WR, Dong SS, Chen EB, Cai JL, Wan JL, Du JX, Song LN, et al. Targeting HNRNPM inhibits cancer stemness and enhances antitumor immunity in wnt-activated hepatocellular carcinoma. *Cell Mol Gastroenterol Hepatol.* 2022;13:1413–47.
21. Wang X, Li J, Bian X, Wu C, Hua J, Chang S, Yu T, Li H, Li Y, Hu S et al. circURI1 interacts with hnRNPM to inhibit metastasis by modulating alternative splicing in gastric cancer. *Proc Natl Acad Sci U S A.* 2021;118.
22. Xu Y, Gao XD, Lee JH, Huang H, Tan H, Ahn J, Reinke LM, Peter ME, Feng Y, Gius D, et al. Cell type-restricted activity of hnRNPM promotes breast cancer metastasis via regulating alternative splicing. *Genes Dev.* 2014;28:1191–203.
23. Ho JS, Di Tullio F, Schwarz M, Low D, Incarnato D, Gay F, Tabaglio T, Zhang J, Wolmann H, Chen L et al. HNRNPM controls circRNA biogenesis and splicing fidelity to sustain cancer cell fitness. *Elife.* 2021;10.
24. Coudert E, Gehant S, de Castro E, Pozzato M, Baratin D, Neto T, Sigrist CJA, Redaschi N, Bridge A. Annotation of biologically relevant ligands in UniProtKB using ChEBI. *Bioinformatics.* 2023;39.

25. Szklarczyk D, Kirsch R, Koutrouli M, Nastou K, Mehryary F, Hachilif R, Gable AL, Fang T, Doncheva NT, Pyysalo S, et al. The STRING database in 2023: protein-protein association networks and functional enrichment analyses for any sequenced genome of interest. *Nucleic Acids Res.* 2023;51:D638–46.
26. Wu T, Hu E, Xu S, Chen M, Guo P, Dai Z, Feng T, Zhou L, Tang W, Zhan L, et al. clusterProfiler 4.0: a universal enrichment tool for interpreting omics data. *Innov (Camb).* 2021;2:100141.
27. Kanehisa M, Furumichi M, Sato Y, Kawashima M, Ishiguro-Watanabe M. KEGG for taxonomy-based analysis of pathways and genomes. *Nucleic Acids Res.* 2023;51:D587–92.
28. Aleksander SA, Balhoff J, Carbon S, Cherry JM, Drabkin HJ, Ebert D, Feuermann M, Gaudet P, Harris NL, Hill DP et al. The gene ontology knowledgebase in 2023. *Genetics.* 2023;224.
29. Wang Y, Xie Z, Kutschera E, Adams JJ, Kadash-Edmondson KE, Xing Y. rMATs-turbo: an efficient and flexible computational tool for alternative splicing analysis of large-scale RNA-seq data. *Nat Protoc.* 2024;19:1083–104.
30. Zhao L, Zhao Y, Yao C, Dai Y, Li Z, Tang Y. MHA, an interactive website for scRNA-seq data of male genitourinary development and disease. *Andrology.* 2023;11:1157–62.
31. Senoo M, Hozoji H, Ishikawa-Yamauchi Y, Takijiri T, Ohta S, Ukai T, Kabata M, Yamamoto T, Yamada Y, Ikawa M, Ozawa M. RNA-binding protein Ptbp1 regulates alternative splicing and transcriptome in spermatogonia and maintains spermatogenesis in concert with Nanos3. *J Reprod Dev.* 2020;66:459–67.
32. Yang Y, Ran J, Liu M, Li D, Li Y, Shi X, Meng D, Pan J, Ou G, Aneja R, et al. CYLD mediates ciliogenesis in multiple organs by deubiquitinating Cep70 and inactivating HDAC6. *Cell Res.* 2014;24:1342–53.
33. Galletta BJ, Jacobs KC, Fagerstrom CJ, Rusan NM. Asterless is required for centriole length control and sperm development. *J Cell Biol.* 2016;213:435–50.
34. Ceyhan Y, Zhang M, Guo J, Sandoval CG, Vacher J, Kaftanovskaya EM, Agoul-nik AI, Agoul-nik IU. Deletion of inositol polyphosphate 4-phosphatase type-II B affects spermatogenesis in mice. *PLoS ONE.* 2020;15:e0233163.
35. Qin X, Hu W, Song W, Grubissich L, Hu X, Wu G, Ferris S, Dobarro M, Halperin JA. Generation and phenotyping of mCd59a and mCd59b double-knockout mice. *Am J Hematol.* 2009;84:65–70.
36. Caroppo E, Castiglioni F, Nerva F, Colpi EM, Gazzano G, Colpi GM. A complete dissection of the whole testicular parenchyma is required in most patients with nonobstructive azoospermia to obtain enough good quality testicular spermatozoa for ICSI. *Andrology.* 2023;11:508–14.
37. Senoo M, Takijiri T, Yoshida N, Ozawa M, Ikawa M. PTBP1 contributes to spermatogenesis through regulation of proliferation in spermatogonia. *J Reprod Dev.* 2019;65:37–46.
38. Miyata H, Shimada K, Kaneda Y, Ikawa M. Development of functional spermatozoa in mammalian spermiogenesis. *Development.* 2024;151.
39. Avidor-Reiss T, Carr A, Fishman EL. The sperm centrioles. *Mol Cell Endocrinol.* 2020;518:110987.

Publisher's note

Springer Nature remains neutral with regard to jurisdictional claims in published maps and institutional affiliations.